

Measuring the Three Point Correlation Function of the Cosmic Microwave Background

Gang Chen¹ and István Szapudi¹

ABSTRACT

We present a new method to estimate three-point correlations in Cosmic Microwave Background maps. Our Fast Fourier Transform based implementation estimates three-point functions using all possible configurations (triangles) at a controlled resolution. The speed of the technique depends both on the resolution and the total number of pixels N . The resulting $N \log N$ scaling is substantially faster than naive methods with prohibitive N^3 scaling. As an initial application, we measure three-point correlation functions in the First Year Data Release of the Wilkinson Anisotropy Probe. We estimate 336 cross-correlations of any triplet of maps from the 8 differential assemblies, scanning altogether 2.6 million triangular configurations. Estimating covariances from Gaussian signal plus realistic noise simulations, we perform a null-hypothesis testing with regards to the Gaussianity of the Cosmic Microwave Background. Our main result is that at the three-point level WMAP is fully consistent with Gaussianity. To quantify the level of possible deviations, we introduce false discovery rate analysis, a novel statistical technique to analyze for three-point measurements. This confirms that the data are consistent with Gaussianity at better than $1\text{-}\sigma$ level when jointly considering all configurations. We constrain a specific non-Gaussian model using the quadratic approximation of weak non-Gaussianities in terms of the f_{NLT} parameter, for which we construct an estimator from the the three-point function. We find that using the skewness alone is more constraining than a heuristic sub-optimal combination of all our results; our best estimate is $f_{NLT} = -110 \pm 150$ assuming a Λ CDM concordance model.

Subject headings: cosmic microwave background — cosmology: theory — methods: statistical

¹Institute for Astronomy, University of Hawaii, 2680 Woodlawn Dr, Honolulu, HI 96822, USA

1. Introduction

The temperature fluctuations in the Cosmic Microwave Background (CMB) are Gaussian to a high degree of accuracy (Komatsu et al. 2003a). Non-Gaussianity, if any, enters at a highly subdominant level. It could be either primordially generated along with Gaussian fluctuations by exotic inflationary models, and/or it could arise from secondary anisotropies, such as gravitational lensing, Sunyaev-Zel’dovich (SZ), or Sachs-Wolfe (SW) effects. Quantifying the degree and nature of non-Gaussianity in the CMB constrains specific inflationary models, as well as enhances our understanding of the secondary processes the CMB underwent beyond the surface of last scattering. Interpretation of any such measurement is complicated by the fact that systematics and foreground contaminations might also produce non-Gaussian signatures.

Given the nearly Gaussian nature of the CMB, N -point correlation functions, and their harmonic counterparts, polyspectra, are the most natural tools for the perturbative understanding of non-Gaussianity. If it were generated by inflationary models admitting a Φ^2 term, the leading order effect would be a 3-point function. On the other hand some secondary anisotropies, such as lensing, are known to produce 4-point non-Gaussianity at leading order (Bernardeau 1997). The skewness (or integrated bispectrum) was measured by Komatsu et al. (2003a) and 3-point correlation function by Gaztañaga & Wagg (2003); Eriksen et al. (2005).

Many alternative statistics have been used to investigate non-Gaussianity in CMB. A partial list includes wavelet coefficients (Vielva et al. 2004; Mukherjee & Wang 2004; Liu & Zhang 2005; McEwen et al. 2005), Minkowski functionals (Komatsu et al. 2003a; Park 2004), phase correlations between spherical harmonic coefficients (Naselsky et al. 2005), multipole alignment statistics (de Oliveira-Costa et al. 2004; Copi et al. 2004; Slosar & Seljak 2004), statistics of hot and cold spots (Larson & Wandelt 2005; Tojeiro et al. 2005; Cruz et al. 2005), higher criticism statistic of pixel values directly (Cayon et al. 2005). Most of these measurements are consistent with Gaussianity, although some claim detections of non-Gaussianity up to $3\text{-}\sigma$ level. These alternative statistics, albeit often easier to measure, typically depend on N -point functions in a complex way, thus they cannot pin-point as precisely the source of non-Gaussianity.

Among the three-point statistics, there is a perceived complementarity between harmonic and real space methods. The bispectrum can be relatively easily calculated for a full sky map (Komatsu et al. 2002), although the present methods have a somewhat slow $N^{5/2}$ scaling (Komatsu et al. 2003b). Methods put forward so far use the “pseudo-bispectrum”, ignoring the convolution with the complicated geometry induced by galactic cut and cut-out holes. In contrast with harmonic space, the corresponding pixel space edge effect correc-

tions are trivial (Szapudi et al. 2001), since the window function is diagonal. Unfortunately, simple methods to measure three-point clustering exhibit a prohibitive N^3 scaling if the full configuration space is scanned. To remedy the situation, most previous measurements of the 3-point function only deal with an ad-hoc sub-set of triangular configurations (Gaztañaga & Wagg 2003; Eriksen et al. 2005). Both of these papers covered the full configuration space on small scales; the former paper also appears to have estimated most configurations on large scales, missing intermediate configurations with mixed scales.

This work presents a novel method, which, at a given resolution, scans the full available configuration space for 3-point level statistics using realistic computational resources. We find that the resulting configuration space itself is overwhelming to such a degree that interpretation of the results also requires novel methods. We introduce false discovery rate (FDR) technique as a tool to interpret three-point correlation function measurements.

The next section introduces our algorithm to measure the 3-point correlation function, §3 illustrates it with an application to the WMAP first year data release, and §4 introduces the FDR method and applies it to our results. We summarize and discuss our results in §5.

2. Measuring the three point correlation function

The three point correlation function (e.g., Peebles 1980) is defined as a joint moment of three density fields $\zeta = \langle \delta_0 \delta_1 \delta_2 \rangle$ at three spatial positions. For CMB studies δ_i denotes temperature fluctuations at position i on the sky, and $\langle \rangle$ stands for ensemble average. If the underlying distribution is spatially isotropic, ζ will only depend on the shape and size of a (spherical) triangle arising from the three positions. A number of characterizations of this triangle are possible and convenient. The most widely used are the sizes of its sides (measured in radians), or two sizes and the angle between them. This latter angle is measured on the spherical surface of the sky.

One can use the ergodic principle of replacing ensemble averages with spatial averages to construct a nearly optimal, edge corrected estimator with heuristic weights (Szapudi & Szalay 1998; Szapudi et al. 2001, 2005)

$$\zeta(\Delta) = \frac{\sum_{i,j,k} f_{i,j,k}^\Delta \delta_i \delta_j \delta_k w_i w_j w_k}{\sum_{i,j,k} f_{i,j,k}^\Delta w_i w_j w_k}, \quad (1)$$

where we symbolically denoted a particular triangular configuration with Δ (any parametrization would suffice), and $f_{i,j,k}^\Delta \propto 1$ if pixels $(i, j, k) \in \Delta$, and 0 otherwise. We also defined a multiplicative weight w_i for each pixel: this is 0 if a pixel is masked out, and it could take various convenient values depending on our noise weighting scheme if the pixel is inside the

survey; e.g., in the case of flat weights it is simply 1. This simple estimator has been widely used in large scale structure, and it is nearly optimal with appropriate weights. (e.g., Szapudi & Szalay 1998; Kayo et al. 2004). It is entirely analogous to the successful estimators used for the measurements of the C_l 's for the CMB (up to harmonic transform, Szapudi et al. 2001; Hivon et al. 2002).

The naive realization of Equation 1 has a prohibitive N^3 scaling if one needs to scan through triplets of pixels and assign them to a particular bin. The summation can be restricted and thus made faster if one restricts the number of configurations and the resolution (e.g., Szapudi et al. 1999b; Barriga & Gaztañaga 2002; Gaztañaga & Wagg 2003), or it can be sped up by using tree-data structures (Moore et al. 2001). Neither of these methods is able to scan through all possible configurations in megapixel maps with reasonable amount of computing resources. Here we propose a new method which uses both hierarchical pixelization and Fourier methods motivated by Szapudi (2004); Szapudi et al. (2005) to scan through all the triangles simultaneously. Note that Gaztañaga & Wagg (2003) comes closest to our aims, but their simple two-step approach is not systematic enough to cover all possible triangles at a given resolution, and it is not fast enough for massive Monte Carlo simulations.

In the following we will choose a parametrization of the triangle Δ using two of its sides θ_1, θ_2 , and the angle α between them. We define the configuration space as a set of (logarithmic) bins for the sides, and linear bins for the angle in their full possible range, i.e., $0, \pi$ (remember that the sides of the triangle on the sky are also measured in radians). The given resolution is determined by the number of bins for θ_i , and the number of bins for α . Note that a particular triangle might appear more than once in this scheme, albeit with different resolutions. Different triangular bins of the three-point function are strongly correlated anyway, and the correlation from duplicating triangles can be taken into account in the general statistical framework over correlated bins.

Given a triangular configuration, and a pixel i , all other pixels which enter the summation in Equation 1 are located on two concentric rings of size θ_1 and θ_2 . As a consequence, the summation over fixed α can be thought of as an unnormalized (raw) two-point correlation function between two rings. To obtain three-point correlation function, one has to multiply this two-point correlation function with the value of the center pixel i and finally sum over i .

Calculating the two-point correlation function of rings can be fast if one repixelizes the map (c.f., Fig. 1) into rings with sizes matching the binning scheme for θ , and uniform division in α . Such a repixelization, resulting in ring-pixels as shown in Fig. 1, would take only N steps even in a naive way; the HEALPix hierarchical scheme allows it to be done in $\log N$ time.

We use the following algorithm: let us start a recursive tree walk at the coarsest map, $N_{side} = 1$ in the HEALPix scheme. For each pixel in this map, we determine, using its center, which ring-pixel it would belong to. If the size of the pixel is much smaller than this ring-pixel (how much smaller is a parameter of our algorithm: in this paper we used the condition that the pixel has to be smaller than $0.2 \times$ the bin width which is also the approximate size of the ring-pixels), we record it. If not, algorithm splits the quad-tree, and calls itself recursively for each four sub-pixels. This procedure ends at the latest when the highest resolution (i.e. the one of the underlying map) is reached. If the bins are chosen appropriately such that large ring-pixels are set up for large triangles, for many pixels it will finish earlier. As noted above, the map has to be regrided around each pixel into rings of ring-pixels. In total, this takes $O(N \log N)$ time.

Calculating the two-point correlation function between rings speeds up using Fast Fourier Transform (FFT) methods, such as those put forward in Szapudi et al. (2001, 2005); Szapudi (2005). The recipe is the following. First, FFT every ring i to obtain complex coefficients $a_k(\theta_i)$; then calculate for every pair of rings (i, j) the “pseudo power spectrum” $a_k(\theta_i)a_k^*(\theta_j) + a_k^*(\theta_i)a_k(\theta_j)$, where $*$ means complex conjugate. Due to the U(1) symmetry of the ring an inverse cos transform will give the (raw) two-point correlation function between the two rings (c.f. Szapudi et al. 2005; Szapudi 2005). If we have N_θ rings, each of them N_α ring-pixels, each FFT can be done in $N_\alpha \log N_\alpha$ time, and there is $N_\theta(N_\theta + 1)/2$ cross correlations to be calculated for a full scan of configurations. All the above needs to be performed for each pixel as a center point. The total scaling (including the initial regriding) takes $N(\log N + N_\theta N_\alpha \log N_\alpha + N_\alpha N_\theta(N_\theta + 1)/4)/2$, where we took into account that the two opposite pixels can be handled in one go if a symmetric set of bins around $\pi/2$ are used for θ .

While the above procedure to calculate raw (unnormalized) correlation functions appears somewhat complex, we have checked with direct calculation that it gives numerically the same result as calculating correlations on the rings in a naive way. In order to obtain normalized correlation functions, the same procedure has to be followed for the rings associated with weights/masks. Each configuration of the raw three-point function is divided with the mask/weight three-point function for the final result. For many realizations with the same mask, such as in the case of massive Monte Carlo simulations, the mask correlations need to be estimated only once, representing negligible cost.

The above abstract scheme and calculation will be illustrated and further clarified with a practical application to WMAP next.

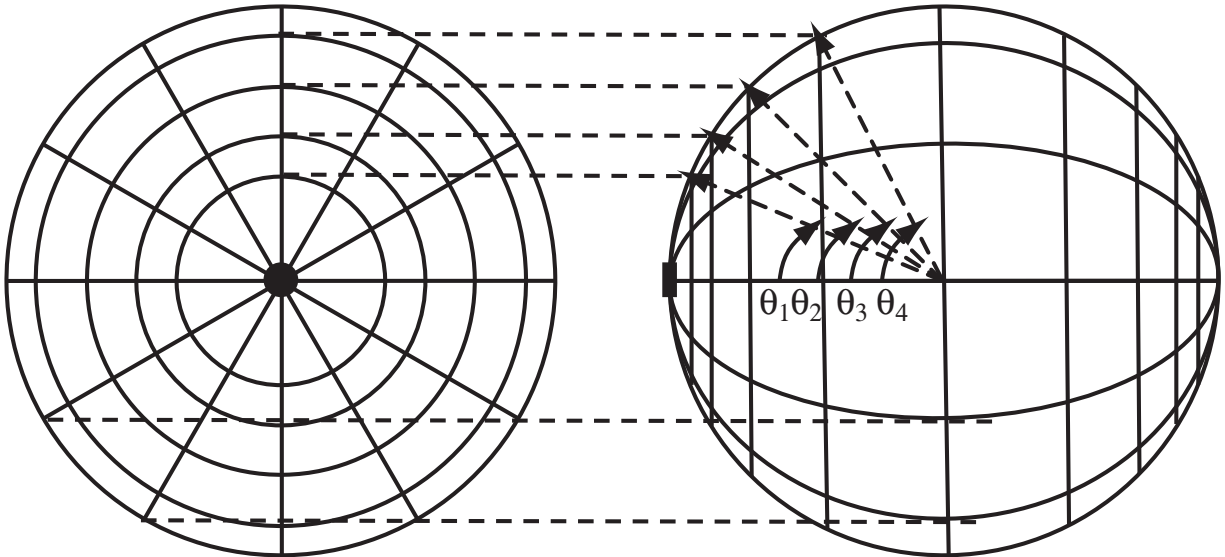


Fig. 1.— The repixellization geometry viewed from position above the center and from the side of the center. θ_i s on the side view define circles on the top view that separate the rings. The radius on the top view corresponding to big circles on the side view that cut rings to the new ring-pixels.

3. Application to WMAP: raw results

3.1. Data and Simulations

We demonstrate our method to calculate the three-point correlation function with an application to WMAP. We downloaded first year foreground cleaned maps from LAMBDA website ¹(Bennett et al. 2003). There are total 8 maps for 8 Differencing Assemblies (DA) in Q, V and W bands: Q1, Q2, V1, V2, W1, W2, W3, and W4, already in HEALPix format. Following the two-point analysis of WMAP (Spergel et al. 2003; Fosalba & Szapudi 2004), we only used cross correlations, i.e. three-point correlation functions calculated from three different DAs.

We produced 100 (Gaussian) simulations with SYNFAST in HEALPix package². The

¹<http://lambda.gsfc.nasa.gov/>

²<http://www.eso.org/science/healpix/>

input power spectrum, also from the LAMBDA website, was taken from Λ CDM model using a scale-dependent (running) primordial spectral index which best fits the WMAP, CBI and ACBAR CMB data, plus the 2dF and Lyman-alpha data. Every simulation consists of 8 assembly maps as the data (Spergel et al. 2003). These 8 maps were generated with a same random seed, representing the same primordial CMB, but 8 different beam transfer functions. Then different simulated noise maps from LAMBDA web (Hinshaw et al. 2003) were added to the SYNFAST output maps.

Since the non-Gaussian signal is exceedingly small, and on the smallest scales the data are noise dominated, we degraded all maps (simulations and data) to $N_{side} = 256$ after applying the kp2 mask. More precisely, we added up pixel and weight values for each map; our two weighting schemes are presented in the next subsection.

3.2. Binning and Weighting

At the heart of our algorithm is the regridding of Figure 1 which matches our binning of the triangles. We chose 19 rings for half of the sphere surface, and the same bins are repeated on the other half symmetrically around $\pi/2$. The 19 bins are chosen to be uniformly distributed in logarithm between $\frac{\pi}{2}/n_{side}$ and $\frac{\pi}{2}$. The number 19 was chosen such that $\theta_{i+1}^2 \simeq 2\theta_i^2$, which gives a logarithmic resolution of $\sqrt{2}$. Every ring was divided to 20 ring-pixels in α . This number renders the resulting ring-pixels fairly compact, and it is also convenient for our chosen implementation of FFT (FFTW, Frigo & Johnson 2005).

Weight maps were constructed using the kp2 mask and the noise profile of the maps. We used two weighting schemes: flat weighting where w_i is 1 or 0 depending on the mask, and (inverse) noise weighting; for the latter (Bennett et al. 2003) we used the effective number of observations of the pixel. The weights need to be determined only up to multiplicative factor, as their overall normalization cancels from the algorithm. The average noise level σ_0 for each DA is used when combining ζ over different cross correlations.

The total number of triangular configurations in 38 rings with 11 possible values of α (angles large than π count to $2\pi - \alpha$) is $38 \times 39/2 \times 11 = 8151$ for autocorrelations. The same number is valid for a cross correlations (which we will be exclusively doing) of 3 DAs. We introduce the notation (DA1, DA2, DA3), for the central pixel, the first ring and the second ring sampled from the three DA in this order. In addition we restrict the “first ring” has θ_i no larger than that of the “second ring”. Then the total number of cross correlations between the 8 DA’s is $8 \times 7 \times 6 = 336$. Effectively, each triangle is calculated six times for a given triplet of DA’s due to the possible 6 permutations. However, each sample has

a different resolution, therefore we opt to keep all possibilities. The resulting correlations are taken into account when dealing with correlated bins in general. In total, there are about 2.6×10^6 triangular configurations for each data or simulation set. Note that the total number of triplets of ring-pixels examined is $20 \times N_{pix}$ more, or 4.4×10^{13} . This is still a lot smaller than checking 10^{18} triplets of pixels naively in an $N_{size} = 256$ map. These numbers suggest that our algorithm even without FFT should take order of days, while the naive algorithm would need over 200 years of CPU.

For a batch of 10 simulations (comprising of 10×8 DA maps), the calculation of the full three-point function in all the configuration takes about 90 hours on an Intel Xeon 2.4GHz CPU. This means each cross-correlation takes only about 2 minutes on average! About 10 hours are saved by batch processing 10 sets of simulations: to estimate ζ in the data alone (one set of 8 DA files) took 10 hours.

Clearly, the given resolution does not extract all the information from the data, as there are approximately $O(N^{3/2})$ distinct configurations of the bispectrum or three-point function. However, it surely must be redundant to extract more configurations than the amount of data. The ratio of data points vs. configurations is about 50 for our chosen bins. It is unlikely that it were fruitful to push this number towards much smaller values, although the speed of our algorithm would allow higher resolution.

3.3. The Three-Point Function of WMAP

Figure 2 shows a typical set of ζ measurements for the (W2,W3,W4) DA cross-correlation. The results from WMAP lie comfortably in the 68% range of results from Gaussian simulations. Similar results are found for the other DA combinations, or when all the 24 possible W-only DA results are averaged. Although different combinations have different effective beam, full averaging is meaningful on large scales. We checked that averaging all 336 possible combinations is also consistent with Gaussian. Finally, repeating all the measurement with noise weighting produced no obvious departure from Gaussianity either.

At the same time, the scatter in the simulations, i.e., the probability density function (PDF) of ζ from 100 simulation, shows a slightly non-Gaussian signature. For (W2,W3,W4), Figure 3 shows a histogram derived from all simulated ζ values normalized by their measured median and 68% levels. Slight deviations from Gaussian distribution are evident: Student distribution of degree 3 fits better the overall distribution. This same distribution produces lower χ^2 when applied to *individual* triangular configurations according to the inset, i.e. it is a (marginally) better fit than Gaussian. We fully take this into account in our hypothesis

testing which is described next.

4. Hypothesis Testing

Our goal is to test the null-hypothesis of Gaussianity against our measurements by means of comparing the ζ values measured from the data with the corresponding probability distribution function (PDF) determined from Gaussian simulations. A crucial step in the traditional χ^2 method appears to be computationally infeasible due to the large number of configurations: calculation of the (pseudo) inverse of an $n \times n$ matrix for $n = 2.6 \times 10^6$, the total number of our highly correlated configurations. Moreover, as seen above, the underlying PDF marginally violates Gaussian assumption, even for Gaussian simulations. Even if it were possible to calculate the inverse of the covariance matrix, and we were to accept the accuracy of the Gaussianity in PDF of the individual bins, it is not possible to determine the underlying covariance matrix with sufficient accuracy. In fact, one would need (e.g., Pan & Szapudi 2005) at least (and likely much more than) 2.6 million simulations for that purpose. Larson & Wandelt (2005) have shown that using simulations with uncorrelated noise might result in spurious detection of non-Gaussianity. Therefore we chose to use only the WMAP supplied correlated noise simulations, of which 110 is available at present.

It is straightforward to test the null-hypothesis with a single configuration: we can calculate a p -value from the best fit Student distribution from our simulations. The p -value is defined as the probability of obtaining a ζ value that is at least as extreme as the one measured from WMAP. For a threshold p_t , the null-hypothesis is rejected at $1 - p_t$ level if the p -value of the datum is smaller than p_t . A problem arises from combining 2.6 million tests when all the data are used. For instance, even if the hypothesis were true, about 260 bins would still be rejected at the 99.99% level (ignoring the correlations in the data).

Fortunately a robust and simple method exists for massive hypothesis testing, which is insensitive to correlations between the tests, and makes no assumption on the Gaussianity of the underlying error distribution: the method of False Discovery Rate (FDR) (Benjamini & Hochberg 1995; Benjamini & Yekutieli 2001). In astronomy, it has been successfully applied in the context of image processing and finding outliers by Miller et al. (2001), which can be consulted for a more detailed introduction. The FDR method combines the same p -value as defined above for individual tests using a threshold for rejecting the null hypothesis. This combination is insensitive to correlations and has more statistical power than naive combination. Our goal is to adapt this powerful method for hypothesis testing of three-point correlation function measurements with overwhelming number of configurations.

The FDR method gives a simple prescription for finding a threshold for rejection. In particular, the recipe suggests that we choose a threshold such that we control the rate of *false rejections* or FDR. The parameter, taking a similar role to the confidence interval in more traditional tests, is the maximum rate of FDR. If we fix an α such that $0 \leq \alpha \leq 1$, the FDR procedure will guarantee

$$\langle FDR \rangle \leq \alpha \tag{2}$$

in ensemble average.

Next we describe the recipe to control FDR; more details can be found in Miller et al. (2001). Let P_1, \dots, P_N denote the p -values calculated from the measurements of N configurations, *sorted* from smallest to largest. Let

$$d = \max \left\{ j : P_j < \frac{j\alpha}{c_N N} \right\} \tag{3}$$

where c_N is a constant depending on the level of correlations between different configurations. For uncorrelated data $c_N = 1$; while $c_N \lesssim \sum_{i=1}^N i^{-1}$ can be used for correlated data (Hopkins et al. 2002). Note that technically one would have to adjust c_N to the degree of correlations in the data. The suggested value for correlated data is extremely conservative, and should be considered as a strong upper limit. Even using this conservative adjustment decreases the statistical power of the technique only logarithmically; the final results are expected to be robust regardless of the degree of correlations.

If configurations with $i < d$ are rejected, Equation 2 will hold (Benjamini & Hochberg 1995), i.e. the FDR is controlled according to our preset parameter α . The procedure is represented graphically on Figure 4: P_j is plotted against j/N superposed with the line through the origin of slope α/c_N . All p -values reject the null hypotheses which are to the left from the last point at which P_j falls below the line. These might include some false discoveries which are guaranteed to be a smaller fraction than α in ensemble average.

4.1. Application the WMAP ζ

We have applied the FDR recipe to all of our individual cross-three point functions, as well as our full data set. Since c_N is a constant, initially we kept $c_N = 1$. For a fixed α , the results can be subsequently reinterpreted in terms of any $c_N > 1$. For DA combination (W2, W3, W4), there is no rejection for $\alpha < 0.81$, i.e., allowing as high as 81% false rejections, not a single configuration rejected our Gaussian null hypothesis. Correlations might increase c_N , but it must be $\lesssim 14$. The true α , when correlations are taking into account, can only

be larger than our effective α for $c_N = 1$. In other words, the data are fully consistent with Gaussianity.

As a sanity check, we repeated the FDR analysis in our simulations as well. By scanning through different α values from 0 to 1, we find that 50 out of 100 simulations have rejections with $\alpha < 0.81$. This means that the WMAP measurements are fully consistent with Gaussianity at a level better than $1-\sigma$ in the traditional sense. In summary, at the three-point level, scanning all configurations, we did not find any significant non-Gaussianity which would be localized in pixel space triangular configurations.

We performed FDR analysis on all 336 measurements individually, as well as on the combination of all those measurements with 2.6 million configurations in total. None of these cases produced credible evidence for non-Gaussianity and all of them were fully consistent with our null hypothesis at $\alpha \sim 0.8$.

5. Summary and Discussions

5.1. Summary

We presented a new method to measure angular three-point correlation functions on spherical maps. We achieve an unprecedented $N \log N$ scaling with a combination of hierarchical and Fourier algorithms. The speed of our technique allows a systematical scan of the full available configuration space at a given resolution. Such speed is especially useful for cross correlations and Monte Carlo simulations, where a vast number of configurations and measurements need to be performed. We have achieved a speed of about 2 minutes per cross correlations, when 336 cross-correlations have been estimated simultaneously in $N_{side} = 256$ HEALPix maps using a single Intel Xeon 2.4GHz CPU. This is to be contrasted with a naive approach, which would have taken about 200 years per cross-correlations; a 20 million fold speed up.

As a first application of our code we analyzed the first year WMAP data along with 100 realistic simulations. We have calculated cross-correlations for about 2.6×10^6 triangular configurations, or about 4.4×10^{13} triplets in total in maps of $N_{side} = 256$ corresponding the 8 DA's. The ratio of pixels/configurations is about 50 for each measurement.

Comparing our measurements from 100 Gaussian simulations with realistic correlated noise, we found WMAP to be comfortably within the 68% percent range for most configurations. Any significant departure from Gaussianity at the three-point level, even if localized in particular triangular configurations, would have shown up clearly in our full scan of the

available configuration space. Our main result is that there is no credible evidence of non-Gaussianity at the three-point level at any of the triangular configurations we examined. As a consequence, if the tentative detection of non-Gaussianity claimed in previous works holds up, it should correspond to either 4-point or higher order correlations, or to spatially localized features which break rotational invariance (e.g., McEwen et al. 2005; Cayon et al. 2005). In contrast with our measurements, all previous studies of higher order statistics used autocorrelations. Comparison of our errorbars with that of Gaztañaga & Wagg (2003) appears to show that this increases the errors by a factor of two (see the discussions below). In addition, many measurements used uncorrelated noise simulations. According to the findings of Larson & Wandelt (2005), this might increase the likelihood of finding spurious non-Gaussianity.

Analysis of our Gaussian simulations revealed that there is a slight non-Gaussianity in the error distribution of individual configurations. This is not surprising, since three-point correlation function is a non-linear construction of the Gaussian random variables (c.f. Szapudi et al. 2000). The error distribution is well fit by a Student distribution with 3 degrees of freedom.

To quantify any possible departure of the overall data set from Gaussianity, we introduced a new technique, FDR, to interpret three-point statistics. This corresponds to an optimized multiple hypothesis testing, and it is insensitive to the unavoidable correlations in the data. All of our FDR tests, whether applied to any of the 336 cross correlations, or the combined data set, were fully consistent with Gaussianity with better than $1-\sigma$. This quantifies our previous assertion based on examination of the individual configurations under the assumption of statistical isotropy.

5.2. Discussions: constraining specific models

The above model independent tests showed that there is no credible evidence of any non-Gaussianity in the data. Next we illustrate how our measurements yield constraints on specific non-Gaussian models. We choose a simple phenomenological model corresponding to the quadratic expansion of the density field in terms of one parameter, f_{NLT} , as put forward by (Gaztañaga & Wagg 2003):

$$\delta = \delta_L + f_{NLT}(\delta_L^2 - \langle \delta_L^2 \rangle). \quad (4)$$

To obtain constraints on this parameter, we construct an estimator for f_{NLT}

$$\tilde{f}_{NLT} = \frac{\zeta(\Delta)/2}{\xi_L(\theta_1)\xi_L(\theta_2) + \xi_L(\theta_1)\xi_L(\theta_3) + \xi_L(\theta_3)\xi_L(\theta_2)} \quad (5)$$

where ζ is our measurement in data or simulation maps. We calculated the two-point correlation function ξ_L analytically, to avoid any bias from the non-linear construction (c.f. Szapudi et al. 1999a). We used the same best fit power spectrum as for the simulations, as well as taking into account beam and pixel window functions. Since previous measurements already established the weakness of non-Gaussianity, our Gaussian simulations should be accurate enough to calculate the variance (Komatsu et al. 2003a). Applying the same estimator to our 100 simulations, we obtained error bars for f_{NLT} estimated from each particular configuration.

The simplicity of the phenomenological model lies in the fact that a constant value of f_{NLT} is assumed. We do not attempt to combine our estimates optimally, instead we use simple considerations. The signal increases towards small scales in this model, while noise dominates on the smallest scales. Since we already discarded the smallest scales when using $N_{size} = 256$, it is intuitively clear that most signal pertaining to this model will be concentrated in the small fraction of the triangles corresponding to small scales, in particular the skewness. To confirm this we generated and analyzed a set of non-Gaussian simulations according to Equation 4, with f_{NLT} equal to 1000, 2000, 3000, 4000, and 6000. Inspection of the configurations together with the errorbars from the Gaussian simulations confirmed the above idea. Therefore we decided to use the skewness, which corresponds to giving zero weight to all other configurations when combining our f_{NLT} estimators. From these we obtain

$$f_{NLT} \sim -110 \pm 150, \tag{6}$$

where the errorbar was estimated from the Gaussian simulations. Gaztañaga & Wagg (2003) quotes similar constraints for a low quadrupole CDM model, but their errorbars are a factor of two larger for a Λ CDM model similar to the one we use. The fact that we obtained a factor of two tighter constraints than Gaztañaga & Wagg (2003) suggests that using cross-correlations is superior to auto-correlations for three-point statistics of WMAP

As a sanity check, we calculated the mean value of the skewness estimator for 100 Gaussian simulations; it yields about $f_{NLT} \simeq -8.0$. On the other hand, we also demonstrate that we can recover f_{NLT} from the non-Gaussian simulations. All the simulations have the same underlying Gaussian signal and noise, the only difference is the value of f_{NLT} . According to Figure 5 the errors might be underestimated when $f_{NLT} > 2000$, and/or there might be a small low bias, but it is clear from the figure that we could detect non-Gaussianity if it were present.

A suboptimal combination of f_{NLT} estimates from all configurations weighted by their inverse variance yields about $f_{NLT} \sim -450 \pm 500$, a significantly weaker result, confirming the intuitive idea that most of the signal is concentrated on small scales.

Some of the results in this paper have been derived using the HEALPix (Górski et al. 1999) package. We acknowledge the use of the Legacy Archive for Microwave Background Data Analysis (LAMBDA). Support for LAMBDA is provided by the NASA Office of Space Science. The authors were supported by NASA through AISR NAG5-11996, and ATP NASA NAG5-12101 as well as by NSF grants AST02-06243, AST-0434413 and ITR 1120201-128440.

REFERENCES

- Barriga, J. & Gaztañaga, E. 2002, *MNRAS*, 333, 443
- Benjamini, Y. & Hochberg, Y. 1995, *J. R. Stat. Soc. B*, 57, 289
- Benjamini, Y. & Yekutieli, D. 2001, *Ann. Stat.*, 29, 1165
- Bennett, C. L., Halpern, M., Hinshaw, G., Jarosik, N., Kogut, A., Limon, M., Meyer, S. S., Page, L., Spergel, D. N., Tucker, G. S., Wollack, E., Wright, E. L., Barnes, C., Greason, M. R., Hill, R. S., Komatsu, E., Nolta, M. R., Odegard, N., Peiris, H. V., Verde, L., & Weiland, J. L. 2003, *ApJS*, 148, 1
- Bernardeau, F. 1997, *A&A*, 324, 15
- Cayon, L., Jin, J., & Treaster, A. 2005, *ArXiv Astrophysics e-prints*
- Copi, C. J., Huterer, D., & Starkman, G. D. 2004, *Phys. Rev. D*, 70, 043515
- Cruz, M., Martínez-González, E., Vielva, P., & Cayón, L. 2005, *MNRAS*, 356, 29
- de Oliveira-Costa, A., Tegmark, M., Zaldarriaga, M., & Hamilton, A. 2004, *Phys. Rev. D*, 69, 063516
- Eriksen, H. K., Banday, A. J., Górski, K. M., & Lilje, P. B. 2005, *ApJ*, 622, 58
- Fosalba, P. & Szapudi, I. 2004, *ApJ*, 617, L95
- Frigo, M. & Johnson, S. G. 2005, *Proceedings of the IEEE*, 93, 216, special issue on "Program Generation, Optimization, and Platform Adaptation"
- Górski, K. M., Hivon, E., & Wandelt, B. D. 1999, in *Evolution of Large Scale Structure : From Recombination to Garching*, 37–+
- Gaztañaga, E. & Wagg, J. 2003, *Phys. Rev. D*, 68, 021302

- Hinshaw, G., Barnes, C., Bennett, C. L., Greason, M. R., Halpern, M., Hill, R. S., Jarosik, N., Kogut, A., Limon, M., Meyer, S. S., Odegard, N., Page, L., Spergel, D. N., Tucker, G. S., Weiland, J. L., Wollack, E., & Wright, E. L. 2003, *ApJS*, 148, 63
- Hivon, E., Górski, K. M., Netterfield, C. B., Crill, B. P., Prunet, S., & Hansen, F. 2002, *ApJ*, 567, 2
- Hopkins, A. M., Miller, C. J., Connolly, A. J., Genovese, C., Nichol, R. C., & Wasserman, L. 2002, *AJ*, 123, 1086
- Kayo, I., Suto, Y., Nichol, R. C., Pan, J., Szapudi, I., Connolly, A. J., Gardner, J., Jain, B., Kulkarni, G., Matsubara, T., Sheth, R., Szalay, A. S., & Brinkmann, J. 2004, *PASJ*, 56, 415
- Komatsu, E., Kogut, A., Nolta, M. R., Bennett, C. L., Halpern, M., Hinshaw, G., Jarosik, N., Limon, M., Meyer, S. S., Page, L., Spergel, D. N., Tucker, G. S., Verde, L., Wollack, E., & Wright, E. L. 2003a, *ApJS*, 148, 119
- Komatsu, E., Spergel, D. N., & Wandelt, B. D. 2003b, *ArXiv Astrophysics e-prints*
- Komatsu, E., Wandelt, B. D., Spergel, D. N., Banday, A. J., & Górski, K. M. 2002, *ApJ*, 566, 19
- Larson, D. L. & Wandelt, B. D. 2005, *ArXiv Astrophysics e-prints*
- Liu, X. & Zhang, S. N. 2005, *ArXiv Astrophysics e-prints*
- McEwen, J. D., Hobson, M. P., Lasenby, A. N., & Mortlock, D. J. 2005, *MNRAS*, 359, 1583
- Miller, C. J., Genovese, C., Nichol, R. C., Wasserman, L., Connolly, A., Reichart, D., Hopkins, A., Schneider, J., & Moore, A. 2001, *AJ*, 122, 3492
- Moore, A. W., Connolly, A. J., Genovese, C., Gray, A., Grone, L., Kanidoris, N., Nichol, R. C., Schneider, J., Szalay, A. S., Szapudi, I., & Wasserman, L. 2001, in *Mining the Sky*, 71–+
- Mukherjee, P. & Wang, Y. 2004, *ApJ*, 613, 51
- Naselsky, P., Chiang, L., Olesen, P., & Novikov, I. 2005, *ArXiv Astrophysics e-prints*
- Pan, J. & Szapudi, I. 2005, *MNRAS*, 361, 357
- Park, C. 2004, *MNRAS*, 349, 313

- Peebles, P. J. E. 1980, *The large-scale structure of the universe* (Research supported by the National Science Foundation. Princeton, N.J., Princeton University Press, 1980. 435 p.)
- Slosar, A. & Seljak, U. 2004, *Phys. Rev. D*, 70, 083002
- Spergel, D. N., Verde, L., Peiris, H. V., Komatsu, E., Nolta, M. R., Bennett, C. L., Halpern, M., Hinshaw, G., Jarosik, N., Kogut, A., Limon, M., Meyer, S. S., Page, L., Tucker, G. S., Weiland, J. L., Wollack, E., & Wright, E. L. 2003, *ApJS*, 148, 175
- Szapudi, I. 2004, *ApJ*, 605, L89
- . 2005, in preparing
- Szapudi, I., Colombi, S., & Bernardeau, F. 1999a, *MNRAS*, 310, 428
- Szapudi, I., Colombi, S., Jenkins, A., & Colberg, J. 2000, *MNRAS*, 313, 725
- Szapudi, I., Pan, J., Prunet, S., & Budavári, T. 2005, *ArXiv Astrophysics e-prints*
- Szapudi, I., Prunet, S., Pogosyan, D., Szalay, A. S., & Bond, J. R. 2001, *ApJ*, 548, L115
- Szapudi, I., Quinn, T., Stadel, J., & Lake, G. 1999b, *ApJ*, 517, 54
- Szapudi, S. & Szalay, A. S. 1998, *ApJ*, 494, L41+
- Tojeiro, R., Castro, P. G., Heavens, A. F., & Gupta, S. 2005, *ArXiv Astrophysics e-prints*
- Vielva, P., Martínez-González, E., Barreiro, R. B., Sanz, J. L., & Cayón, L. 2004, *ApJ*, 609, 22

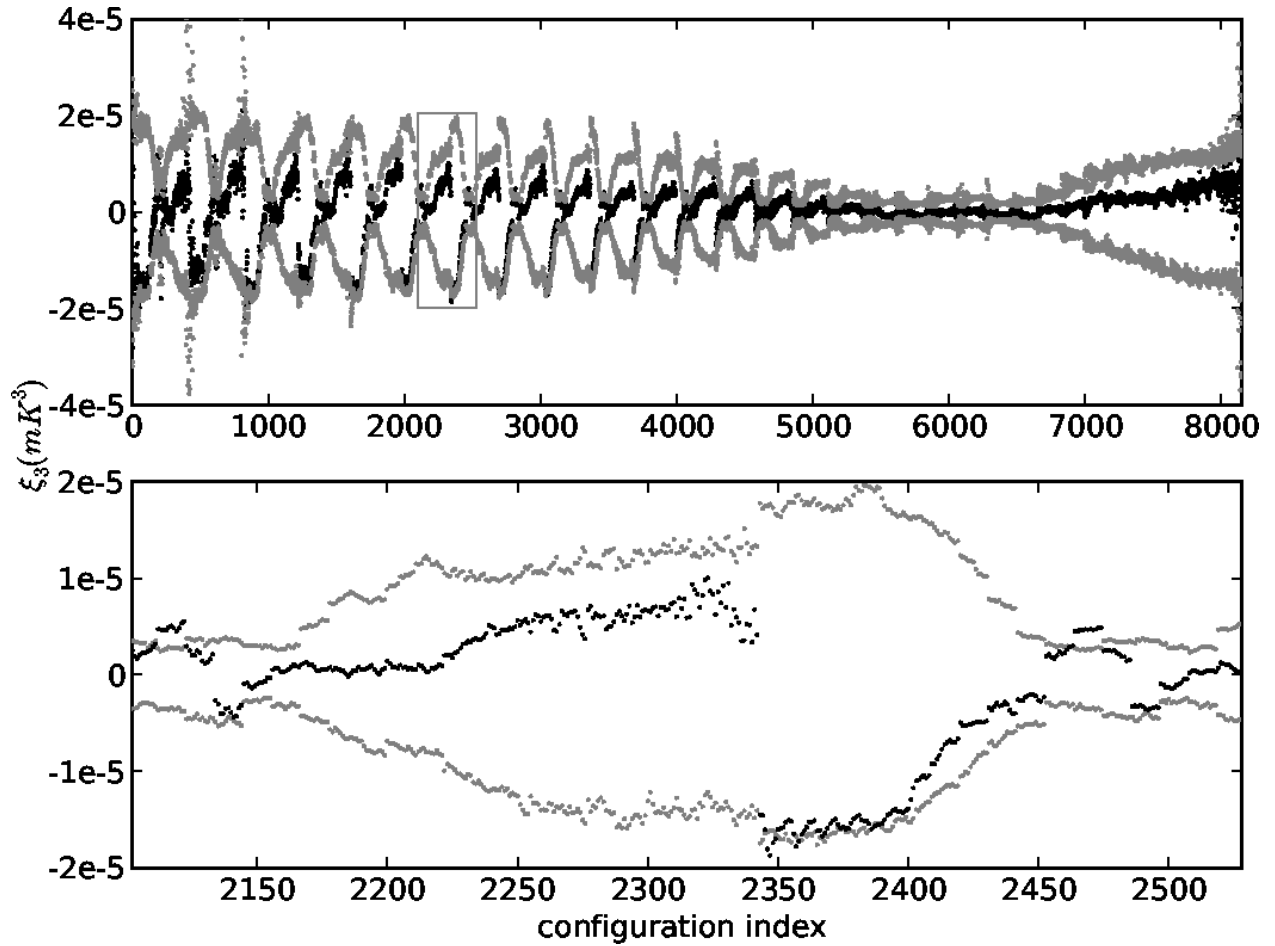


Fig. 2.— ζ values of all 8151 configurations for the cross correlation (W2,W3,W4). Top: the light gray points show the middle 68% range estimated from 100 Gaussian simulations, the dark gray points correspond to ζ from WMAP. Bottom: zoom on the details inside the small box in the top.

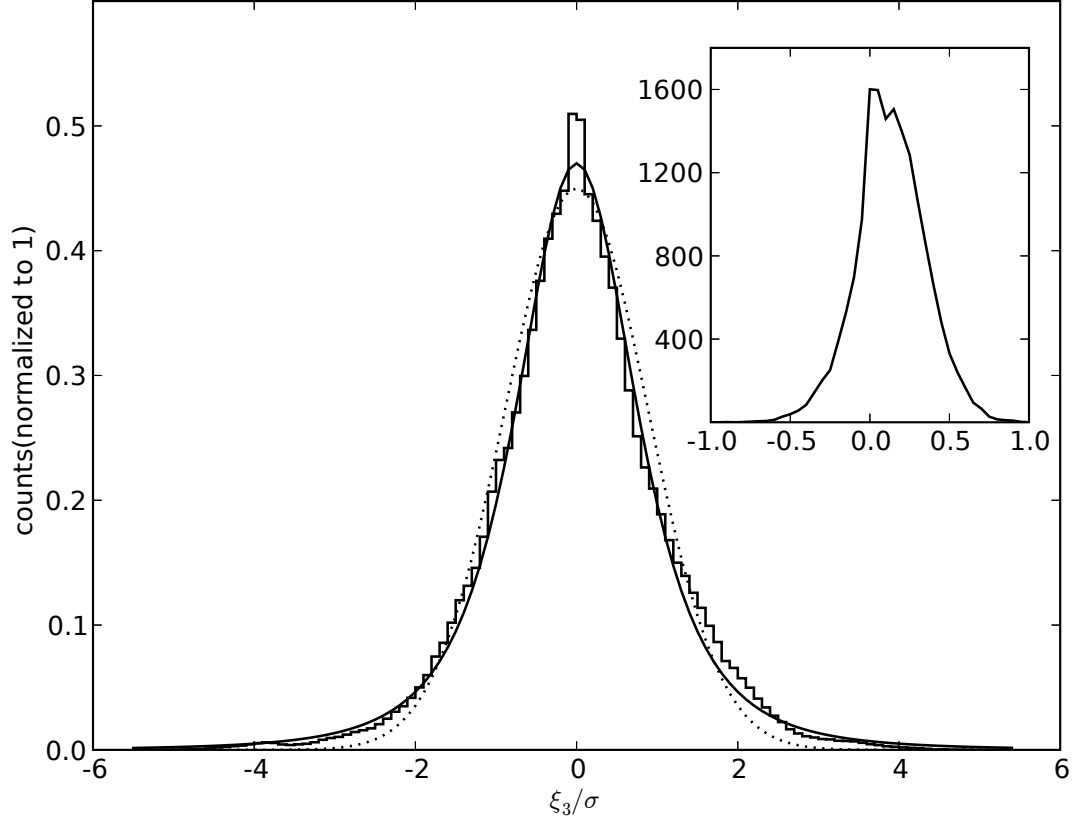


Fig. 3.— Histogram of ζ values of all 100 simulations for all configurations in (W2, W3, W4). Each value has been renormalized by subtracting the median, and divided with σ calculated from 68 percentiles. The two curves correspond to best fitting Gaussian (dots) and Student function (solid line) with 3 degrees of freedom. *Inset*: histogram of χ^2 differences between fitting a Gaussian or Student distribution for each bin. According to the figure, most configurations are better fitted by a Student distribution as evidenced by the larger χ^2 for the former; however, Gaussian is still a reasonable fit.

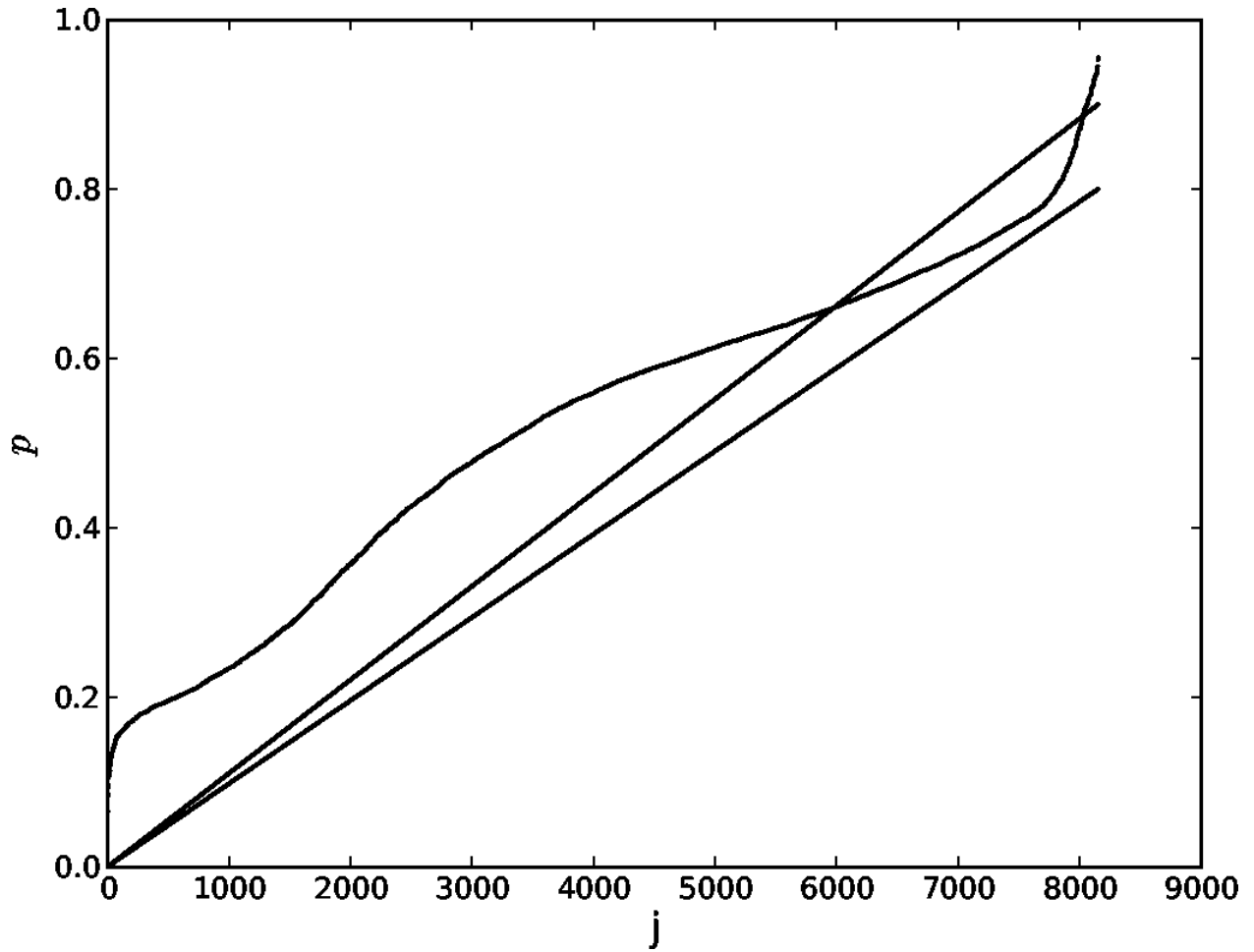


Fig. 4.— The sorted p values vs. lines with slope α/c_N . The p values shown in the curve are for all configurations of our typical DA combination ($W2, W3, W4$). The lower line is for $\alpha = 0.8$ and produces no rejection. On the other hand, the upper line is for $\alpha = 0.9$ produces many (8000) rejections, probably all of them false discoveries (see text).

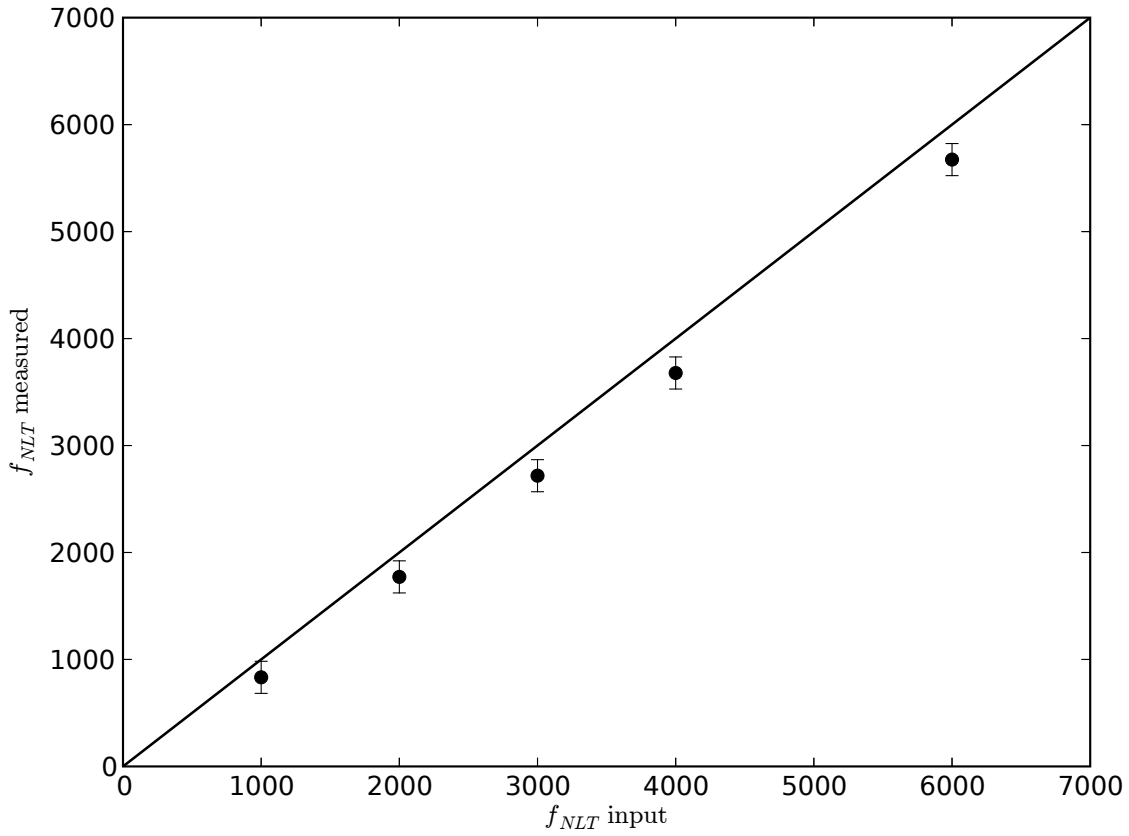


Fig. 5.— Comparing the measured f_{NLT} values, using skewness, with the input f_{NLT} values for the non-Gaussian simulations. The straight line represents the input values. The points with error bars are the measured values. All the error bars are the same value from 100 Gaussian simulations.